Regular Article

PHYSICAL CHEMISTRY RESEARCH
Published by the
Iranian Chemical Society
www.physchemres.org
info@physchemres.org

Phys. Chem. Res., Vol. 9, No. 3, 447-465, September 2021
DOI: 10.22036/pcr.2021.260496.1863

Extraction, Characterization and Methyl Orange Sequestration Capacity of Cellulose Nanocrystals Derived from Sugarcane Bagasse: Experimental and Regression Modelling

L. Azeez[a,*], A.L. Adejumo[b], A.O. Oyedeji[c], S.A. Adebisi[a] and H.K. Busari[a]

[a]*Department of Pure and Applied Chemistry, Osun State University, Osogbo, Nigeria*
[b]*Department of Chemical Engineering, Osun State University, Osogbo, Nigeria*
[c]*Department of Science Laboratory Technology, Federal Polytechnic Ilaro, Nigeria*
(Received 4 December 2020, Accepted 6 March 2021)

The adsorption capacity of cellulose nanocrystals extracted from sugarcane bagasse using acid hydrolysis for methyl orange (MO) sequestration was investigated. The extracted nanocrystals were characterized by scanning electron microscopy (SEM), energy dispersive X-ray (EDX) and Fourier transform infra-red spectroscopy (FTIR). The cellulose nanocrystals were well identified by their features including well-defined pore spaces, predominant nano range of particles (0.045-0.082 μm), greater crystallinity index from 1.09 to 1.21, disappearance of peaks at 1736 and 1429 cm^{-1} in FTIR, and higher carbon content. A Two-fold improvement in monolayer adsorption capacity was obtained for cellulose nanocrystals (432.17 mg g^{-1}), described by Langmuir isotherm, and for bagasse (170.99 mg g^{-1}), described by Freundlich isotherm. Adsorption processes on both adsorbents were spontaneous, exothermic and followed pseudo-second order kinetics. Polynomial regression models appropriately predicted equations through which the effects of different batch adsorption parameters on MO removal were described, even with descriptions better than the experimentally generated data.

Keywords: Adsorption capacity, Sugarcane bagasse, Cellulose nanocrystals, Exothermic, Polynomial regression model

INTRODUCTION

Quality water is indispensable, yet it is difficult to come by due to an increase in the population-needing comfort coupled with the establishment of micro-industrial scale companies that generate wastes [1-3,68]. Wastes generated at homes, companies and industries eventually find their ways into surface water thus degrading its quality [64,66]. Waste generation is expected to continue as the population continues to rise and more industries are created. Most pollutants that found their way into water bodies are non-biodegradable, recalcitrant, stable to oxidation and are as dangerous as their intermediates [4-6,63,75]. Methyl orange (MO) is a complex azo-structured anionic dye that has found usefulness in laboratories, photography and textile but its discharge in water has been reported to interrupt ecological balance along with disruption of water quality parameters [66,70]. Exposure to wastewater containing MO has been epidemiologically linked with adverse health effects on humans and death of aquatic lives. MO is known to be carcinogenic, teratogenic and mutagenic [7-10,64]. The presence of chromophoric -N=N- in the structure of MO makes wastewater containing MO usually difficult to remediate. Hence, to meet the people's water demands, holistic approaches must be employed to remove highly toxic MO [70,75].

Several methods ranging from flocculation, coagulation, adsorption, biological degradation, membrane filtration, electrochemical and reverse osmosis are in use for wastewater remediation [63,67]. Adsorption has been a frequently applied remediation method due to its simplicity and other encouraging attributes [3,11,12,62,65]. However,

*Corresponding author. E-mail: luqman.azeez@uniosun.edu.ng

contending with drawbacks associated with some of the aforementioned methods and high-cost of many adsorbents, different studies have reported applications of inexpensive and readily available adsorbents particularly activated carbons from waste materials [63,68]. These are also not without limitations as typically used adsorbents are macro-scaled, and therefore, large quantities would be needed to achieve excellent results [13,14,72,74].

Meanwhile, progression in nanotechnology has made remediation a lot easier owing to the intrinsic characteristics of nanostructured materials that possess enhanced adsorptive properties as against macro-scaled materials. Additionally, their inexpensive, renewable, biodegradable, retentive and regenerative properties are encouraging to dismiss together with using small quantities to achieve greater adsorption results [15-17,71,73].

Nanocellulose is a decomposable, inexhaustive, non-hazardous and environmentally-compliant adsorbent possessing greater reactive sites for environmental remediation [18,19]. Nanocellulose having a diameter of less than 100 nm has found usefulness in medicine, food and construction applications in addition to the environmental remediation of wastes due to its biocompatibility, tensile strength, abundant hydroxyl groups, large surface area and low toxicity [20-26]. It has been deployed for remediating dyes, volatile organic compounds, polycyclic aromatic hydrocarbons, heavy metals and pollutants of their likes [4,26,10,27].

Nanocellulose is obtainable from cellulosic materials by modifying the crystallinity degree without disruption of functional group reactivities but rather with enhanced structural activities accompanied by improved morphological assemblage [4,10]. Nanocellulose has been prepared from commonly available, abundant, cost-effective and renewable cellulosic materials such as corncob, corn straw, pineapple leaf, cassava bagasse, cotton, soy hulls, sago pith, kenaf core, rice straw, cocoa bean shell, bamboo, wood, banana leaf, newspaper, jute leaf, groundnut shell, wheat straw, sugarcane bagasse and flax fibre [6,10,17,19, 27,30-36].

Nanocellulose (cellulose nanocrystals) extracted by acid hydrolysis treatment has been extensively explored and are considered easier compared with other methods of nanocellulose synthesis. The acid hydrolysis method is fast, easy and extracts nanocellulose with a high degree of crystallinity and smaller sizes [17,18,28,29]. Therefore, the acid hydrolysis method was chosen in the study.

Sugarcane bagasse is a lignocellulosic fibrous residual waste from sugarcane (*Saccharum officinarum)* after sequencing its juice. It is generally available and litters the environment carelessly in Nigeria. It contains cellulose (45-55%), hemicellulose (25-35%) and lignin (18-24%) and serves as a major raw material for biodiesel production [37]. The high proportion of cellulose in sugarcane bagasse implies its predominant crystallinity and allows for modification of amorphous region. It has been used as an adsorbent for dyes, heavy metals and pesticides due to its richness in carboxyl, phenolic and hydroxyl groups essential for adsorption [36,38,39]. However, most studies reported the application of modified sugarcane bagasse or produced activated carbon from it. Though they were found to be effective as adsorbents, the additional cost of production and modification limit these processes [40].

Extraction of nanocellulose from sugarcane bagasse is a better alternative owing to non-disruption of inherent chirality, available functional groups, biodegradability and biocompatibility with large surface area, enhanced surface functionality and adsorptive properties [6,10,17].

Considering the attendant toxicities that follow the discharge of MO into water sources, the necessity to remediate wastewater containing this dye to ensure environmental sustainability is a focal target. Owing to environmental friendliness, biodegradability, vastly functional surfaces, ease of regeneration, economic viability and ease of extraction coupled with inherent high crystallinity as largely reported by many authors, nanocellulose is a promising adsorbent. Moreover, sugarcane bagasse is an easy source of renewable biowastes produced in large quantities.

Therefore, due to novel properties of nanocellulose, and its wide applications, this study was primarily aimed at extracting nanocellulose from sugarcane bagasse using acid hydrolysis as an economically viable alternative adsorbent for the simulated dye wastewater remediation and predicts model equations that best describe the adsorption process using polynomial regression analysis.

MATERIALS AND METHODS

Sugarcane units were purchased at Oja-Oba market,

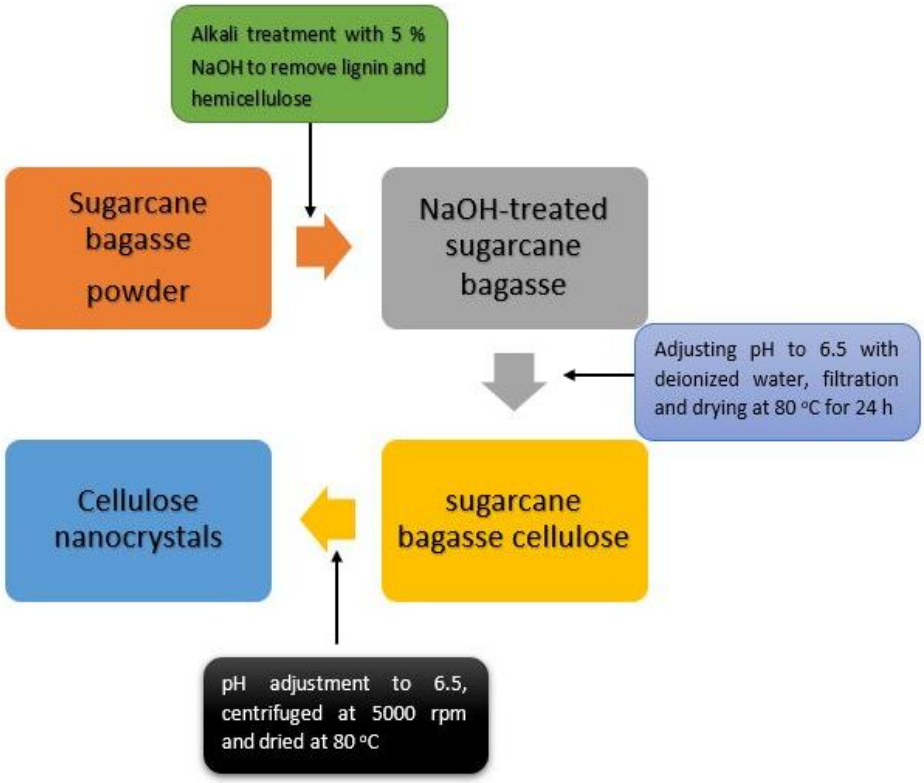

Fig. 1. Scheme for the extraction of cellulose nanocrystals from sugarcane bagasse.

Osogbo, Osun State, Nigeria. Sugarcane units were washed, peeled and its juice was extracted to leave residual bagasse. The residual bagasse was air-dried, milled to powder and oven-dried at 80 °C for 5 h. The powdered sugarcane bagasse was sieved with 425 µm mesh and kept in a tight container for further use. All chemicals (NaOH, H_2SO_4, methyl orange) used were of analytical grade.

Extraction of Cellulose Nanocrystals and Characterization

The extraction method described by Adejumo *et al.* [10] was followed and is illustrated in Fig. 1. Fourier transform infrared spectroscopy (FTIR) (Model 500, Buck Scientific Inc.) was recorded in the range of 400-4000 cm^{-1} with a resolution of 4 cm^{-1} for functional group properties. Scanning electron microscopy coupled with energy dispersive X-ray was done with Jeol JSM-6400 for morphology and elemental composition.

Adsorption Studies

Methyl orange preparation and batch adsorption. Precisely 100 mg l^{-1} of MO was prepared, and different concentrations ranging from 10-50 mg l^{-1} were used for the adsorption study. The influence of operational variables on the sequestration of MO on bagasse and cellulose nanocrystals were studied. Sequestration study was performed by varying initial solution pH from 2 to 10, initial MO concentrations from 10 to 50 mg l^{-1}, bagasse and cellulose nanocrystal dosages from 0.1 to 0.5 g, contact time from 0 to 75 min as well as temperature from 303 to 315 K. Batch adsorption was performed with 0.5 g of each adsorbent added to 50 mg l^{-1} MO in a conical flask placed in a water bath with shaker (Uniscope water bath shaker) thermostatically regulated at 303 K for 30 min and agitated at 300 rpm for all parameters but adsorbent dosage. Absorbance values were recorded at 480 nm using Jenway 6405 UV-Vis spectrophotometer (Buch Scientific Inc.

USA). The percentage sequestration of MO and quantity of MO adsorbed at a particular time were calculated using Eqs. (1) and (2), respectively.

For determination of pH point of zero charges (pH_{pzc}), 0.1 g of each adsorbent was added to 0.1 M NaCl solution (200 ml) of known pH, and the pH was adjusted between 2 and 10 with HCl and NaOH.

$$\%MO\ removal = \frac{(C_i - C_f) \times 100}{C_i} \tag{1}$$

$$q_t = \frac{(C_i - C_t)V}{M} \tag{2}$$

Where q_t is the amount of MO adsorbed per unit mass of adsorbent (mg g^{-1}) at time t, C_i is the initial MO concentration (mg l^{-1}), C_f is the final MO concentration (mg l^{-1}), C_t is the concentration of MO remaining at time t, V is the volume of MO solution (l), and M is the mass of adsorbent (g).

Adsorption Isotherms

Four adsorption isotherms, Eqs. (3) to (6b), were used to fit the equilibrium parameters between MO and adsorbents. The suitability of each model was predicted by comparing correlation coefficients (R^2); the closer it is to unity, the better it is for the description of an isotherm model.

Langmuir isotherm [41]:

$$\frac{C_e}{q_e} = \frac{C_e}{q_{\max}} + \frac{1}{q_{\max} K_L} \tag{3}$$

$$R_L = \frac{1}{1 + K_L C_0} \tag{3a}$$

Freundlich isotherm [42]:

$$\log q_e = \frac{1}{n} \log C_e + \log K_f \tag{4}$$

Tempkin isotherm [43]:

$$q_e = B \ln A + B \ln C_e \tag{5}$$

$$B = \frac{RT}{b} \tag{5a}$$

Dubinin-Radushkevich [44]:

$$\ln q_e = \ln q_0 - \beta \varepsilon^2 \tag{6}$$

$$\varepsilon = RT \ln\left(1 + \frac{1}{C_e}\right) \tag{6a}$$

$$E = \frac{\sqrt{1}}{2\beta} \tag{6b}$$

where C_e is the equilibrium concentration of MO (mg l^{-1}), q_e is the quantity of MO adsorbed at equilibrium (mg g^{-1}), q_{max} is the maximum monolayer adsorption capacity (mg g^{-1}), K_L is the Langmuir adsorption constant (l mg^{-1}), R_L is the Langmuir separation, K_f is the Freundlich constants for binding energy, n is the adsorption intensity, b (J mol^{-1}) is the heat of absorption, and E is the energy of adsorption.

Adsorption Kinetics

The kinetic models studied for fitting the adsorption kinetics are listed in Eqs. (7), (8) and (9). The adsorption mechanism was studied with intra-particle diffusion (Eq. (10)). The suitability of each model for describing kinetic models was validated with correlation coefficient (R^2) and non-linear Chi-square test (Eq. (11)).

Pseudo first-order kinetics:

$$\ln(q_e - q_t) = \ln q_e - K_1 t \tag{7}$$

Pseudo second-order kinetics:

$$\frac{t}{q_t} = \frac{1}{K_2 q_{e^2}} + \frac{t}{q_e} \tag{8}$$

Elovich kinetics:

$$q_t = \frac{1}{\beta} \ln(\alpha\beta) + \frac{1}{\beta} \ln t \tag{9}$$

$$q_t = K_{diff} t^{\frac{1}{2}} + C \tag{10}$$

$$\chi^2 = \sum_{i=1}^{n} \frac{(q_{\exp} - q_{cal})^2}{q_{cal}} \tag{11}$$

where q_e^- is the quantity adsorbed at equilibrium (mg g^{-1}), q_t is the quantity adsorbed at time t (mg g^{-1}), K_1 is the rate constant for the pseudo first order (min^{-1}), K_2 is the rate constant of the pseudo second order (g mg^{-1} min^{-1}), K_{diff} is the rate constant of intraparticle diffusion (mg g^{-1} $min^{-1/2}$), α is the chemisorption rate, and β is the extent of surface coverage.

Adsorption Thermodynamics

Parameters to describe adsorption thermodynamics were obtained from Eqs. (12) and (13).

$$\ln K_0 = \frac{\Delta S^\circ}{R} - \frac{\Delta H^\circ}{RT} \tag{12}$$

$$\Delta G^\circ = \Delta H - T\Delta S \tag{13}$$

ΔS° is change in entropy, ΔH° is change in enthalpy and ΔG° is change in free energy

Regeneration Studies

Precisely, 0.1 g of each of sugarcane bagasse and cellulose nanocrystals was added to separate 50 ml of 50 mg l^{-1} MO in a 250 ml flask. The solutions were adjusted to pH 3 and 6 (pH of maximum adsorption) for sugarcane bagasse and cellulose nanocrystals, respectively, and subsequently agitated for 1 h. After that, the solutions were centrifuged at 300 rpm for 30 min and residual MO concentration was determined at 480 nm. Methyl orange-loaded adsorbents were washed with water, dried at 70 °C to complete dryness and then soaked in 100 ml water for the desorption process. This mixture was shaken vigorously for 30 min, centrifuged and desorbed MO concentration from methyl orange-loaded adsorbents was determined. Percentage desorption was calculated using Eq. (14)

$$Percentage\ desorption = \frac{Quantity\ of\ dye\ desorbed\ by\ water}{Quantity\ adsorbed\ during\ loading} \times 100 \tag{14}$$

Polynomial Regression Prediction of Adsorption Process

Data generated from adsorption isotherms, kinetics and thermodynamics were fitted to polynomial linear regression to predict optimum conditions that best describe the adsorption of MO on bagasse and cellulose nanocrystals. The polynomial regression model for prediction was based on Eq. (15) where a set of *x* interaction variables is modelled to obtain dependent *y*. The predictive agreement between experimentally generated and model-predicted data was determined using correlation coefficient R^2 and statistical significance at 95% confidence level. The predicted equations and validations for all experimental data are presented along with each batch adsorption parameter.

$$y = \beta_0 + \beta_1 x + \beta_2 x^2 \tag{15}$$

where β_0, β_1, β_2 are intercepts of model

RESULTS AND DISCUSSION

Characterization of Bagasse and Cellulose Nanocrystals

Scanning electron microscopy coupled with EDX was used to study the morphological arrangement, particle size and elemental compositions of bagasse (Fig. 2a) and extracted cellulose nanocrystals (Fig. 2b). Diameters of particles of bagasse range between 2.0 and 6.4 μm with predominant particles with sizes between 3.1 and 4.2 μm (insert). Cellulose nanocrystals have particles in the range 0.045-0.193 μm predominantly between 0.045 and 0.082 μm (insert). The SEM image of bagasse shows a more compressed morphology while the SEM image of cellulose nanocrystal reveals a better porous morphology. These ranges and characteristics indicate that nanostructure morphology of cellulose nanocrystals is vital for adsorption processes [25,27,45,46].

Cellulose nanocrystals contain higher weight percentage of carbon, silicon and a lower percentage of oxygen compared to bagasse as obtained in EDX results (Figs. 2a and 2b). This implies better adsorption properties of the cellulose nanocrystals since the adsorption capacity is a function of the carbon content [36,47,61].

To study the surface chemistry of both adsorbents, FTIR characterization spectra (Fig. 3) reveal major functional groups in bagasse (BG) and cellulose nanocrystals (NBG). Peaks at 3414 and 1053 cm^{-1} in BG and 3418 and 1047 cm^{-1} in NBG indicate stretching vibrations of OH and

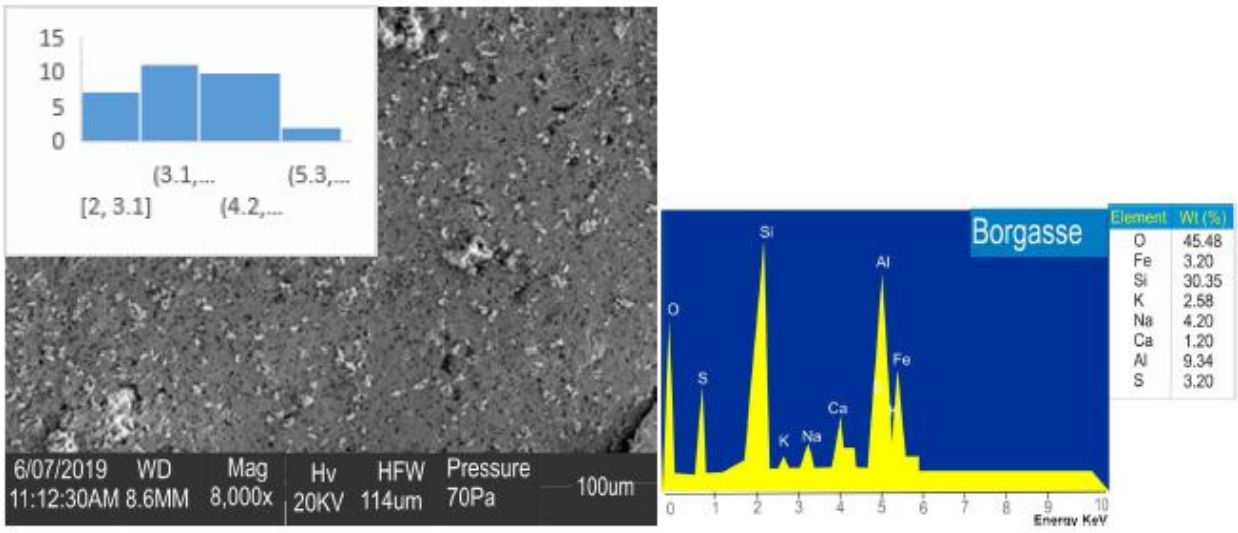

Fig. 2a. SEM image and elemental composition of sugarcane bagasse.

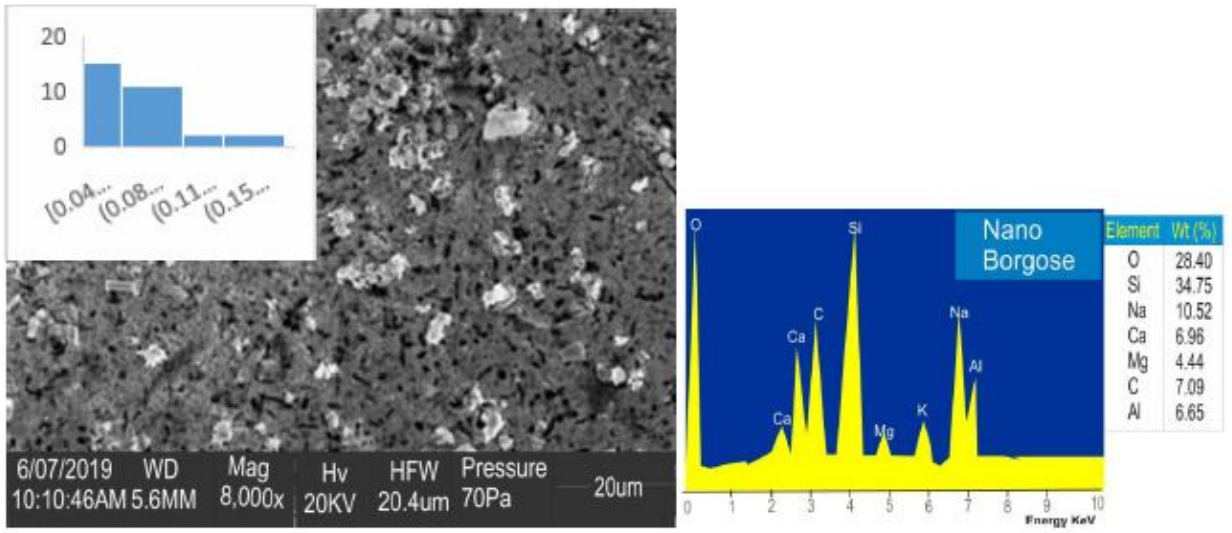

Fig. 2b. SEM image and elemental composition of the cellulose nanocrystals.

asymmetric cellulosic bridges of C-O-C groups, respectively. Peaks from 2897 to 2941 cm^{-1} in both adsorbents correspond to C-H of methyl and methylene. Peaks at 1736 and 1429 cm^{-1} imply the presence of uronic and acetyl C=O from lignin and hemicellulose, respectively, in BG which disappeared in cellulose nanocrystals. This implies a more crystalline cellulosic material in cellulose nanocrystals since hemicellulose and lignin are the amorphous regions in lignocellulose [17,19]. The appearance of the peak at 1121 cm^{-1} in cellulose nanocrystals attributed to SO_4^{2-} is an attestation of H_2SO_4 hydrolysis [18]. Peaks between 1600-1638 cm^{-1} correspond

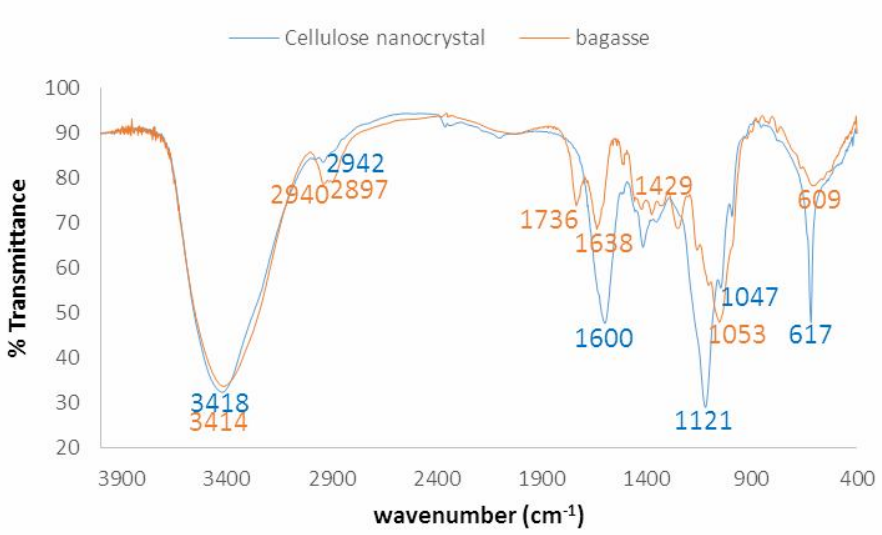

Fig. 3. FTIR spectra of cellulose nanocrystals and sugarcane bagasse.

to the bending vibrations of OH associated with adsorbed water.

Peaks in BG and NBG spectra are representative of lignocellulose and nanocellulose reported in the literature. Moreover, the FTIR characterization indicates the retention of inherent cellulosic nature of BG in cellulose nanocrystals with complete removal of lignin and hemicellulose [6,10,17,19,36,37,39,48].

Further analysis of FTIR data on crystallinity index, degree of the disordered region and hydrogen bonding pattern were explored. The total crystallinity index (CI) was determined as the ratio of absorbance intensities of crystalline bands at 1373 to 2900 cm^{-1} while the lateral order index (LOI) is the ratio of 1433 to 895 cm^{-1} proposed by Hurtubise and Krassig [49] and Nelson and O' Connor [50]. The energy of hydrogen bonding (E_H) is described by Equation 16. Crystallinity index and energy of hydrogen bonding are parameters to assess orderliness/crystallinity of a cellulosic material [19,51,52]

$$E_H = \frac{1}{K} \times \left(\frac{\nu_0 - \nu}{\nu_0} \right) \quad (16)$$

where k is 1.68E-2, ν_0 and ν are frequencies of free hydrogen bonded OH (3600 cm^{-1}) and hydrogen bonded OH, respectively.

The increase in values of CI, LOI and E_H from 1.09 to 1.21, 1.23 to 1.33 and 27.96 to 29.17 kcal, respectively imply an improvement in structural crystallinity and regularity of cellulose nanocrystals over bagasse. The results aligned with the work of Bano and Negi [19] and Kruer-Zerhusen *et al.* [52]. The increased crystallinity index is connected to the removal of amorphous regions of hemicellulose and lignin during NaOH treatment as obtained in FTIR and better ordered crystalline region due to the formation of new hydrogen bonds [6,53].

Effects of Different Parameters on Batch Adsorption Studies

The surface charges of adsorbents play a prominent role in the adsorption process. As obtained for both adsorbents, pH points of zero charge (pH_{pzc}) of cellulose nanocrystals and bagasse were 4.1 and 8.3, respectively. At these values (pH_{pzc}), both adsorbents had zero net charge while they were positively charged at pH < pH_{pzc} and negatively charged at pH > pH_{pzc}. As expected, maximum removal of MO on these adsorbents occurred at pH 3 and 6 for cellulose nanocrystals and bagasse, respectively (Fig. 4). Adsorption maximum attained at these pH values was due to the electrostatic interaction between cationic surfaces of adsorbents (cationic at pH < pH_{pzc}) and anionic MO [8,54,55,63,69,74]. There was an initial increase in the

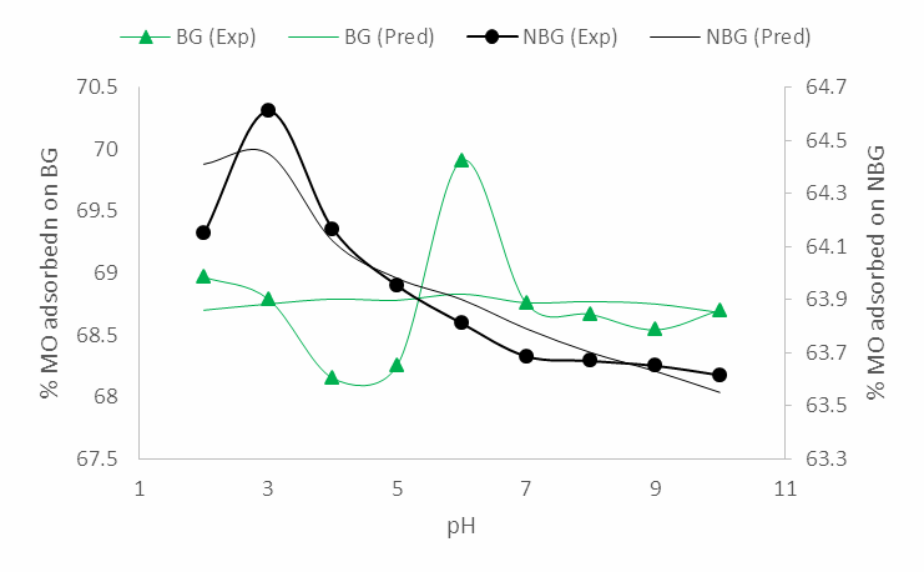

Fig. 4. Effects of pH on percentage adsorption of MO and model prediction.

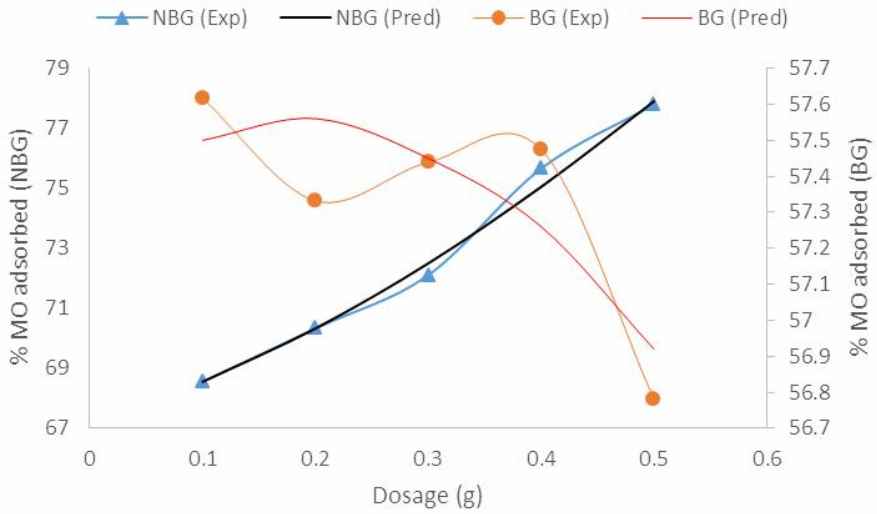

Fig. 5. Effects of dosage on percentage adsorption of MO and model prediction.

percentage removal of MO on cellulose nanocrystals from pH 2 to 3 and after that, it dropped considerably till pH 10 while there was a gradual decrease in the percentage removal of MO on bagasse from pH 2 to 5 followed by an increase at pH 6 and thereafter dropped until pH 10.

The prediction of effects of pH on percentage removal of MO modelled with polynomial regression follows Eqs. (17a) and (17b) for bagasse and cellulose nanocrystals, respectively. The accuracy was high (R^2 = 0.928) with insignificant variations, although with lower percentages between experimentally and predicted percentages of MO removal on cellulose nanocrystals (Fig. 4). Conversely, the agreement between experimentally and predicted percentages of MO removal on bagasse (Fig. 4) was pointedly low (R^2 = 0.015).

$$y = 68.59 + 0.071x - 0.006x^2 \qquad (R^2 = 0.015,\ p = 0.985) \tag{17a}$$

$$y = 64.75 - 0.188x - 0.007x^2 \qquad (R^2 = 0.928,\ p = 0.072) \tag{17b}$$

Percentage uptake of MO on different dosages of cellulose nanocrystals increased from 69-78% whereas a slight reduction in the percentage of adsorption on bagasse with an increase in dosage from 57.6-56.8% was obtained (Fig. 5). The increase in percentage adsorption recorded for nanocrystals may be connected to the available larger surface area and more reactive sites for MO uptake. Conversely, a slight reduction in the percentage of uptake on bagasse could be due to the compactness of bagasse layers [47,56,57]. Model equations of polynomial regression for predicting effects of dosage on the percentage removal of MO are given as 18a and 18b for bagasse and cellulose nanocrystals, respectively. The model-predicted similar trends of a strong agreement without significant difference for cellulose nanocrystals and an average correlation with significant disparities for bagasse between model predicted and experimentally generated data (Fig. 5).

$$y = 57.34 + 0.228x - 0.006x^2 \qquad (R^2 = 0.57,\ p = 0.43) \tag{18a}$$

$$y = 66.99 + 1.31x + 0.178x^2 \qquad (R^2 = 0.99,\ p = 0.01) \tag{18b}$$

Percentage sequestration of MO decreased with increase in the concentration of MO from 59.75 to 18.67% for cellulose nanocrystals and 51.08 to 6.63% for bagasse (Fig. 6) from the lowest (10 mg l^{-1}) to the highest (50 mg l^{-1}) concentrations of MO. These reductions are related to the saturation of vacant reactive sites and pore spaces on both adsorbents [55,56]. At low concentration, the ratio of MO molecules to reactive sites of adsorbent was smaller hence higher percentage. However, as the MO concentrations increased, the ratio of MO molecules adsorbed to vacant reactive sites increased thus the lower percentage. The results are in agreement with Ojo *et al.* [54] and Anitha *et al.* results [58]. The model predicted equations for initial concentrations of MO on bagasse and cellulose nanocrystals are given in Eqs. (19a) and (19b), respectively. Strong correlations with no significant differences between the experimental and model data were obtained for both adsorbents. Regression models predicted an increase in the percentage of MO adsorbed with respect to the initial concentrations on bagasse (Fig. 6)

$$y = 80.80 - 29.94x + 2.52x^2 \qquad (R^2 = 0.89,\ p = 0.11) \tag{19a}$$

$$y = 73.22 - 20.64x + 1.86x^2 \qquad (R^2 = 0.98,\ p = 0.022) \tag{19b}$$

The rate of adsorption with time was initially swift then became gradual until equilibrium was fulfilled at 45 and 35 min for nanocrystals and bagasse, respectively (Fig. 7). This trend of swift uptake of MO could be attributed to the initial driving force of MO to overcome the resistance of mass transfer and availability of vacant reactive sites on both adsorbents occupied as time progressed [47,59,60,62]. Regression of model-predicted equilibrium was attained at 20 and 15 min for bagasse and nanocrystals, respectively, following Eqs. (20a) and (20b). The values of predicted model had significant correlations with experimental data with no significant variations.

$$y = 75.57 + 1.37x - 0.03x^2 \qquad (R^2 = 0.94,\ p = 0.06) \tag{20a}$$

$$y = 81.72 + 1.19x - 0.03x^2 \qquad (R^2 = 0.98,\ p = 0.022) \tag{20b}$$

Effects of temperature on the MO uptake on both adsorbents were detailed between 303-323 K (Fig. 8). The adsorption percentage decreased slightly with increase in temperature from 74.58 to 74.55% for nanocrystals and 74.51 to 74.45% for bagasse. These reductions are an indication of the exothermic nature of the adsorption process [47,59]. The regression of prediction model varied not much significant, that is in close agreement between the experimental and predicted data on effects of temperature on adsorption processing following Eqs. (21a) and (21b) for bagasse and nanocrystals, respectively (Fig. 8).

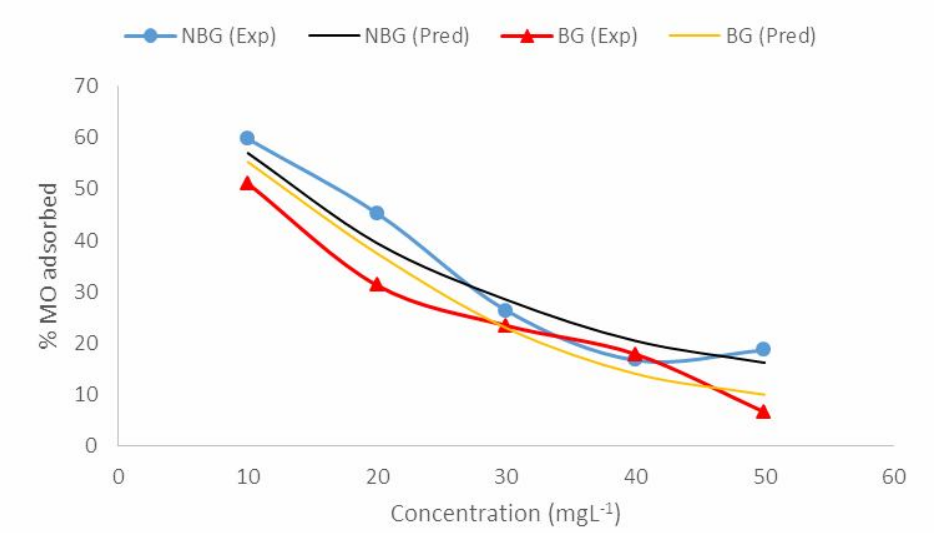

Fig. 6. Effects of initial concentration of MO on percentage adsorption and model prediction.

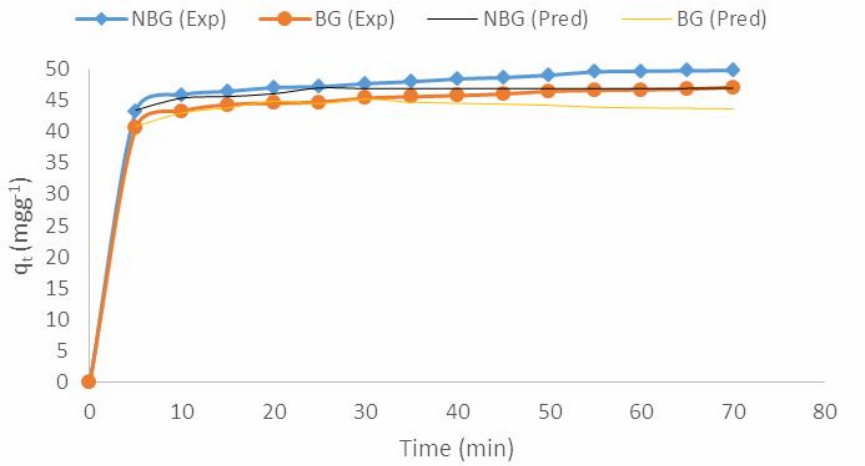

Fig. 7. Quantity of MO adsorbed with respect to time and model prediction.

$$y = 74.63 + 0.0028x - 0.0021x^2 \quad (R^2 = 0.98,\ p = 0.022) \tag{21a}$$

$$y = 74.54 - 0.01x + 0.001x^2 \quad (R^2 = 0.99,\ p = 0.011) \tag{21b}$$

Adsorption Isotherms Study

Adsorption data were fitted to Langmuir, Freundlich, Tempkin and Dubinin-Radushkevich isotherms to investigate the appropriateness of each isotherm describing the adsorption process (Table 1). The appropriateness was determined using the correlation coefficient (R^2) closeness to unity; the closer to unity it is, the better it is for describing the adsorption process [63,65,70].

The suitability of each isotherm for the adsorption process on bagasse is in the order (R^2); Freundlich (0.92) > Dubinin-Radushkevich (0.91) > Langmuir (0.66) > Temkin (0.64). The order of fitting of isotherm model (R^2) for

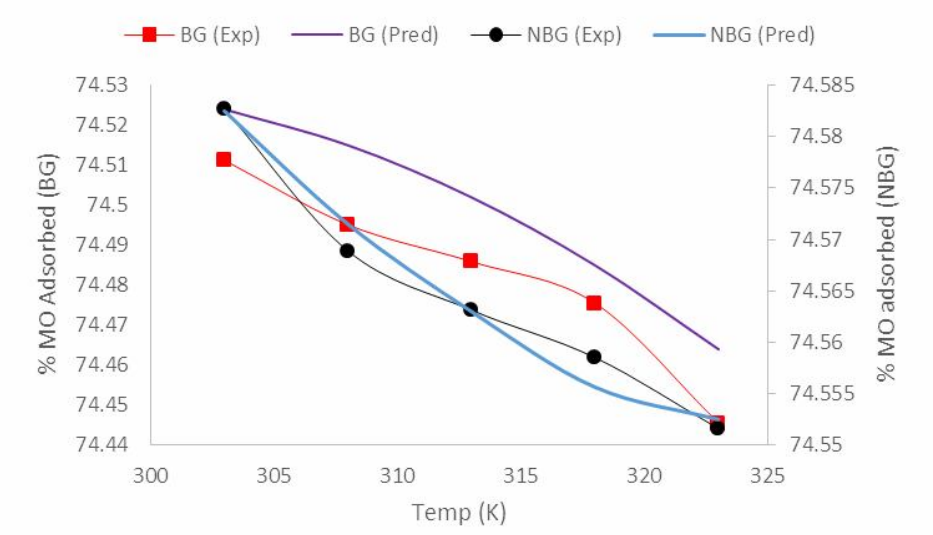

Fig. 8. Effects of temperatures on percentage adsorption of MO and prediction model.

Table 1. Isotherm Parameters for Adsorption of MO on Bagasse and Cellulose Nanocrystals

Isotherms	Parameters	Bagasse (Exp.)	Bagasse (Pred.)	Cellulose nanocrystals (Exp.)	Cellulose nanocrystals (Pred.)
Langmuir	q_{max} (mg g^{-1})	170.99	246.12	432.17	437.06
	K_L (l mg^{-1})	0.013	0.012	1.29	1.30
	R_L	0.595	0.633	0.015	0.015
	R^2	0.66	0.94	0.91	0.996
Freundlich	n	10.21	16.29	5.92	5.68
	K_f	253.72	306.66	231.45	229.07
	R^2	0.92	0.41	0.60	0.74
Temkin	B	29.34	34.92	55.38	59.76
	A (l g^{-1})	8827.1	1115.48	56.81	34.92
	b (J mol^{-1})	85.85	72.15	45.49	42.15
	R^2	0.64	0.57	0.56	0.74
Dubinin Radushkevich	q_o (mg g^{-1})	364.21	332.67	420.44	420.05
	B × 10^{-6} (mol^2 k^{-1} J^{-2})	0.68	0.47	2.01	1.65
	E (kJ mol^{-1})	18.59	20.26	14.98	15.50
	R^2	0.91	0.81	0.61	0.98

cellulose nanocrystals follows Langmuir (0.91) > Dubinin-Radushkevich (0.61) > Freundlich (0.60) > Temkin (0.56). Langmuir and Freundlich were the most appropriate isotherms to describe the adsorption on cellulose nanocrystals and bagasse, implying adsorption on the crystalline uniform surface of cellulose nanocrystals while it was on the heterogeneous surface for bagasse [61,67,68]. The aforementioned observations are in accordance to the results of crystallinity indices calculated for both adsorbents.

Polynomial regression model predicted for both adsorbents was governed by the Langmuir isotherm as obtained in correlation coefficients (R^2_{NBG} - 0.996, R^2_{BG} - 0.94) while improved correlation coefficients (R^2) were predicted for cellulose nanocrystals in Freundlich (0.74), Temkin (0.74) and Dubinin-Radushkevich (0.98) isotherms decrease in R^2 values as predicted for bagasse in Freundlich (R^2 = 0.41), Temkin (0.57) and Dubinin-Radushkevich (0.81) isotherms.

The maximum monolayer adsorption capacity (q_{max}) calculated from Langmuir isotherm for bagasse and cellulose nanocrystals are 170.99 and 432.17 mg g^{-1}, respectively. This is a 2-fold improvement in adsorption capacity of cellulose nanocrystals over bagasse. This is linked to higher carbon content and porosity in nanocrystals [10,67]. Regression analysis predicted a marginal increase in q_{max} for nanocrystals (437.06 mg g^{-1}) and sizeable increase for bagasse (246.12 mg g^{-1}). Comparing q_{max} values of cellulose nanocrystals with the previously reported values in other studies for methyl orange removal (Table 2), cellulose nanocrystals show a far better adsorption performance for MO sequestration.

The parameter to determine favourability of adsorption process (R_L) was found to be 0.0153 and 0.0151 for nanocrystals, and 0.595 and 0.533 for bagasse from experimental and predicted data, respectively. This is an indication of favourable adsorption process [3,13,14,61, 64,70].

Adsorption intensity (n) from Freundlich isotherm model is a hint for explaining favourable (n > 1) or cooperative (n < 1) adsorption process. Values of n calculated were 5.92 and 5.68 for nanocrystals and 10.21 and 16.29 for bagasse from experimental and model-predicted data, respectively. These values validate the favourability of sequestration of MO on both adsorbents [59,60,68].

Adsorption energies that help determine the nature of adsorption process calculated were 14.98 and 15.50 kJ mol^{-1} for nanocrystals and 18.59 and 20.26 kJ mol^{-1} for bagasse from experimental and predicted data, respectively. These values suggest chemisorption as the adsorption mode [3,13,14,72].

Adsorption Kinetic Study

Adsorption kinetic data were fitted and explained using pseudo first order, pseudo second order and Elovich kinetics. The prediction ability of each model was adjudged suitable using correlation coefficient (R^2) and non-linear Chi-square (χ^2) based on comparatively higher R^2 and lower χ^2. The order of accuracy for predicting adsorption kinetics follows pseudo second order (R^2_{NBG} - 0.999, R^2_{BG} - 0.999) > Elovich (R^2_{NBG} - 0.978, R^2_{BG} - 0.983) > pseudo first order (R^2_{NBG} - 0.969, R^2_{BG} - 0.941). Pseudo second order kinetic model was appropriately the best model to predict the kinetics of MO adsorption on both adsorbents as shown by the correlation coefficient, non-linear Chi-square and close agreement between experimental q_e and calculated q_e (Table 3). This validates the domination of the adsorption process by chemisorption as calculated from the adsorption energy [6,11,55,69]. Regression model for predicting adsorption kinetics follows a similar trend for experimental data with improved correlation coefficients.

Adsorption mechanism was studied using Weber and Morris intraparticle diffusion to determine the rate-determining step and the influence of the mass transfer resistance on MO adsorption [54,69]. Intra-particle diffusion displays a rapid step related to the rate-controlling steps and stable step describing the rate-limiting step (Fig. 9). The rapid step explains the diffusion of MO onto the surfaces of adsorbents while the stable step designates the preponderance of intra-particle diffusion in the adsorption process. Two-stage plots with deviations from origin submit that intra-particular diffusion mechanism was involved in the adsorption process but not the sole rate-determining step [3,60].

Table 2. Comparison of the Monolayer Adsorption Capacities of Selected Adsorbents for Methyl Orange Adsorption

Adsorbent	q_{max} (mg g^{-1})	Concentration (mg l^{-1})	Temperature (°C)	Ref.
NiO nanoparticles	370.37	1000	60	Darwish *et al.* [27]
CuO nanoparticles	217.39	1000	60	Darwish *et al.* [27]
Coffee grounds activated carbon	658.00	300	30	Rattanapan *et al.* [9]
Modified chitosan magnetic adsorbent	758.00	100	25	Yang *et al.* [35]
Nitrogen-doped porous carbons	337.80	400	50	Sun *et al.* [76]
Chitosan microspheres	207.00	60	30	Zhai *et al.* [77]
Chitosan/diatomite	35.12	50	20	Zhao *et al.* [6]
Corncob nanocellulose	206.62	50	30	Adejumo *et al.* [10]
Sugarcane bagasse	170.99	50	30	This study
Bagasse cellulose nanocrystals	432.17	50	30	This study

Table 3. Adsorption Kinetics of MO on Different Adsorbents

	Constants	Bagasse (Exp.)	Bagasse (Pred.)	Cellulose nanocrystals (Exp.)	Cellulose nanocrystals (Pred.)
q_e experimental (mg g^{-1})		46.61	45.22	49.67	47.08
Pseudo first order	$q_{e,}$ calculated (mg g^{-1})	16.22	17.40	16.51	15.18
	K_1 (min^{-1})	0.05	0.11	0.04	0.09
	R^2	0.941	0.967	0.969	0.98
	χ^2	2.59	1.92	2.86	3.38
Pseudo second order	$q_{e,}$ calculated (mg g^{-1})	47.50	43.97	50.52	47.27
	K_2 (g mg^{-1} min^{-1})	0.017	0.056	0.014	0.054
	R^2	0.999	0.999	0.999	0.999
	χ^2	0.016	0.035	0.014	0.0008
Elovich	α (mg g^{-1} min^{-1})	57.51	98.21	54.77	77.55
	β (g mg^{-1})	0.45	1.07	0.43	0.81
	R^2	0.967	0.989	0.989	0.99
Intra-particle diffusion	K_{1diff} (mg g^{-1} $min^{-1/2}$)	1.45	1.27	1.64	1.13
	K_{2diff} (mg g^{-1} $min^{-1/2}$)	0.88	0.49	0.88	0.01
	R_1^2	0.86	0.90	0.91	0.88
	R_2^2	0.97	0.98	0.99	0.53

Table 4. Thermodynamic Parameters of MO Adsorption

Adsorbent	ΔH°	ΔS°	ΔG°				
	(kJ mol^{-1})	(J $K^{-1}mol^{-1}$)	(kJ mol^{-1})				
			303 K	306 K	309 K	312 K	315 K
Bagasse (Exp.)	-128.88	41.02	-12.56	-12.76	-12.97	-13.17	-13.38
Bagasse (Pred.)	-128.07	41.03	-12.56	-12.76	-12.97	-13.17	-13.38
Cellulose nanocrystals (Exp.)	-62.51	41.27	-12.57	-12.77	-12.98	-13.19	-13.39
Cellulose nanocrystals (Pred.)	-65.30	41.26	-12.57	-12.72	-12.98	-13.19	-13.39

Adsorption Thermodynamic Study

The values of ΔH°, ΔS° and ΔG° indicating energetics and spontaneity of the adsorption process of MO on bagasse and nanocrystals were evaluated from thermodynamic parameters (Table 4).

Negative values of ΔH° imply the exothermic nature of the adsorption process of MO on both adsorbents with reduced randomness as shown by positive ΔS° values signifying the direct interaction between adsorbate and adsorbents [10,56]. The values of ΔG° ranged from -12.57 to -13.39 kJ mol^{-1} that reduced with increasing temperature. These indicate a spontaneous adsorption process at all temperatures, but more favourably feasible at a higher temperature [11,61]. Regression model predicted approximately the same magnitude of energetic terms and spontaneity of the adsorption process

Regeneration Studies of MO on Adsorbents

Desorption percentages were 79.42 and 83.07% in bagasse and cellulose nanocrystals, respectively. These high percentages indicate that the regeneration of both adsorbents would be easy and suitable for more adsorption processes [61]. This result aligns with the result of the adsorption energy that implies MO molecules were more chemically attracted to bagasse than nanocellulose [10].

CONCLUSIONS

Cellulose nanocrystals using acid hydrolysis method were successfully extracted from sugarcane bagasse, characterized and investigated for their adsorption capacity for methyl orange removal. The disappearance of uronic ester peak of hemicellulose/lignin indicated nanocellulose extraction, while higher carbon content, greater crystallinity index, nano range of particles and larger porosity are parameters that better defined cellulose nanocrystals. A two-fold improvement in monolayer adsorption capacity was obtained for cellulose nanocrystals over bagasse. Adsorption processes were best described by Langmuir isotherm on nanocrystals, whereas Freundlich isotherm was best suited for bagasse. Adsorption processes on both adsorbents were spontaneous, exothermic and best fitted to pseudo second order kinetics. Polynomial regression model appropriately predicted equations that well describe the effects of different batch adsorption parameters on MO removal with better fitting than the experimentally generated data.

REFERENCES

[1] Assouline, S.; Russo, D.; Silber, A; Or, D., Balancing water scarcity and quality for sustainable irrigated agriculture. *Water Resour. Res.* **2015**, *51*, 3419-3436. https://doi.org/10.1002/2015WR017071.

[2] Azeez, L.; Salau, A. K.; Adewuyi, S. O.; Osineye, S. O.; Tijani, K. O.; Balogun, R. O., Safety evaluation of Osun river water containing heavy metals and volatile organic compounds (VOCs) in rats. *Niger. J. Physiol. Sci.* **2015**, *30*, 103-109.

[3] Azeez, L.; Lateef, A.; Adejumo, A. L.; Adeleke, T.

A.; Adetoro, R. O.; Mustapha, Z., Adsorption behaviour of rhodamine B on hen feather and corn starch functionalized with green synthesized silver nanoparticles (AgNPs) mediated with cocoa pod extracts. *Chem. Afr.* **2020**, *3*, 237-250. https://doi.org/10.1007/s42250-019-00113-7.

[4] Jiang, F.; Dinh, D. M.; Hsieh, Y. L., Adsorption and desorption of cationic malachite green dye on cellulose nanofibril aerogels. *Carbohydr. Polym.* **2017**, *173*, 286-294. https://doi.org/10.1016/j.carbpol.2017.05.097.

[5] Gautam, P. K.; Singh, A.; Misra, K.; Sahoo, A. K.; Samanta, S. K., Synthesis and applications of biogenic nanomaterials in drinking and wastewater treatment. *J. Env. Manag.* **2019**, *231*, 734-748. https://doi.org/10.1016/j.jenvman.2018.10.104.

[6] Zhao, P.; Zhang, R.; Wang, J., Adsorption of methyl orange from aqueous solution using chitosan/diatomite composite. *Water Sci. Technol.* **2017**, *75*, 1633-1642. https://doi.org/10.2166/wst.2017.034.

[7] Keyhanian, F.; Shariati, S.; Faraji, M.; Hesabi, M., Magnetite nanoparticles with surface modification for removal of methyl violet from aqueous solutions. *Arab. J. Chem.* **2016**, *9*, S348-S354. https://doi.org/10.1016/j.arabjc.2011.04.012.

[8] Huang, R.; Liu, Q.; Huo, J.; Yang, B., Adsorption of methyl orange onto protonated crosslinked chitosan. *Arab. J. Chem.* **2017**, *10*, 24-32. https://doi.org/10.1016/j.arabjc.2013.05.017.

[9] Rattanapan, S.; Srikram J.; Kongsune, P., Adsorption of methyl orange on coffee grounds activated carbon. *Energy Procedia*. **2017**, *138*, 949-954. https://doi.org/10.1016/j.egypro.2017.10.064.

[10] Adejumo, A. L.; Azeez, L.; Oyedeji, A. O.; Adetoro, R. O.; Aderigbigbe, F. A., Nanostructured and surface functionalized corncob as unique adsorbents for anionic dye remediation. *SN Appl. Sci.* **2020**, *2*, 301. https://doi.org/10.1007/s42452-020-2109-5.

[11] Munagapati, V. S.; Wen, J. -C.; Pan, C. -L.; Gutha, Y.; Wen, J. -H., Enhanced adsorption performance of Reactive Red 120 azo dye from aqueous solution using quaternary amine modified orange peel powder. *J. Mol. Liq.* **2019**, *285*, 375-385. https://doi.org/10.1016/j.molliq.2019.04.081.

[12] Pavithra, K. G.; Kumar, P. S.; Jaikumar, V.; Rajan, P. S., Removal of colorants from wastewater: A review on sources and treatment strategies. *J. Ind. Eng. Chem.* **2019**, *75*, 1-19. https://doi.org/10.1016/j.jiec.2019.02.011.

[13] Azeez, L.; Lateef, A.; Adebisi, S. A.; Oyedeji, A. O., Novel biosynthesized silver nanoparticles from cobweb as adsorbent for rhodamine B: Equilibrium isotherm, Kinetic and Thermodynamic studies. *Appl. Water Sci.* **2018**, *8*, 32. https://doi.org/10.1007/s13201-018-0676-z.

[14] Azeez, L.; Adejumo, A. L.; Asaolu, S. S.; Adeoye, M. D.; Adetoro, R. O., Functionalization of rice husk with *ortho*-phosphoric acid enhanced adsorptive capacity for anionic dye removal. *Chem. Afr.* **2020**, *3*, 457-467. https://doi.org/10.1007/s42250-020-00142-7.

[15] Suman, S.; Kardam, A.; Gera, M.; Jain, V. K., A novel reusable nanocomposite for complete removal of dyes, heavy metals and microbial load from water based on nanocellulose and silver nano-embedded pebbles. Environ. Technol. 2015, 36, 707-714. https://doi.org/10.1080/09593330.2014.959066.

[16] Mahfoudhi, N.; Boufi, S., Nanocellulose as a novel nanostructured adsorbent for environmental remediation: a review. *Cellulose.* **2017**, *24*, 1171-1197. https://doi.org/10.1007/s10570-017-1194-0.

[17] Theivasanthi, T.; Christma, F. L. A.; Adeleke, J. T.; Subash, C. B. G.; Ravichandran, R., Synthesis and characterization of cotton fiber-based nanocellulose. *Int. J. Biol. Macromol.* **2018**, *109*, 832-836. https://doi.org/10.1016/j.ijbiomac.2017.11.054.

[18] Nechyporchuk, O.; Belgacem, M. N.; Bras, J., Production of cellulose nanofibrils: A review of recent advances. *Ind. Crops Prod.* **2016**, *93*, 2-25. https://doi.org/10.1016/j.indcrop.2016.02.016.

[19] Bano, S.; Negi, Y. S., Studies on cellulose nanocrystals isolated from groundnut shells. *Carbohydr. Polym.* **2017**, *157*, 1041-1049. https://doi.org/10.1016/j.carbpol.2016.10.069.

[20] Dufresne, A., Nanocellulose: A new ageless bionanomaterial. *Mater. Today.* **2013**, *16*, 220-227. https://doi.org/10.1016/j.mattod.2013.06.004.

[21] Hosseinidoust, Z.; Alam, M.; Sim, G.; Tufenkji, N.; van de Ven, T., Cellulose nanocrystals with tunable surface charge for nanomedicine. *Nanoscale.* **2015**, 7, 16647-16657. https://doi.org/10.1039/c5nr02506k.

[22] Jorfi, M.; Johan, F. E., Recent advances in nanocellulose for biomedical applications. *J. Appl. Polym. Sci.* **2015**, *132*, 1-19. https://doi.org/10.1002/app.41719.

[23] Abitbol, T.; Rivkin, A.; Cao, Y.; Nevo, Y.; Abraham, E.; Ben-Shalom, T.; Lapidot, S.; Shoseyov, O., Nanocellulose, a tiny fiber with huge applications. *Curr. Opin. Biotechnol.* **2016**, *39*, 76-88. https://doi.org/10.1016/j.copbio.2016.01.002.

[24] Hakkarainen, T.; Koivuniemi, R.; Kosonen, M.; Escobedo-Lucea, C.; Sanz-Garcia, C.; Vuola, J.; Valtonen, J.; Tammela, P.; Mäkitie, A.; Luukko, K.; Yliperttula, M.; Kavola, H., Nanofibrillar cellulose wound dressing in skin graft donor site treatment. *J. Control Release.* **2016**, *244*, 292-301. https://doi.org/10.1016/j.jconrel.2016.07.053.

[25] Phanthong, P.; Reubroycharoen, P.; Hao, X.; Xu, G.; Abudula, A.; Guan, G., Nanocellulose: Extraction and application. *Carbon Resour. Convers.* **2018**, *1*, 32-43. https://doi.org/10.1016/j.crcon.2018.05.004.

[26] Wang, J.; Liu, X.; Jin, T.; He, H.; Liu, L., Preparation of nanocellulose and its potential in reinforced composites: A review. *J. Biomat. Sci. Polym.* **2019**, *30*, 919-946. https://doi.org/10.1080/09205063.2019.1612726.

[27] Darwish, A. A. A.; Rashad, M.; AL-Aoh, H. A., Methyl orange adsorption comparison on nanoparticles: Isotherm, kinetics, and thermodynamic studies. *Dyes Pigm.* **2019**, *160*, 563-571. https://doi.org/10.1016/j.dyepig.2018.08.045.

[28] Yang, X.; Liu, H.; Han, F.; Jiang, S.; Liu, L.; Xia, Z., Fabrication of cellulose nanocrystal from Carex meyeriana Kunth and its application in the adsorption of methylene blue. *Carbohydr. Polym.* **2017**, *175*, 464-472. https://doi.org/10.1016/j.carbpol.2017.08.007.

[29] Yang, X.; Han, F.; Xu, C.; Jiang, S.; Huang, L.; Liu, L.; Xi, Z., Effects of preparation methods on the morphology and properties of nanocellulose (NC) extracted from corn husk. *Ind. Crops Prod.* **2017**, *109*, 241-247. https://doi.org/10.1016/j.indcrop.2017.08.032.

[30] Jonoobi, M.; Oladi, R.; Davoudpour, Y.; Oksman, K.; Dufresne, A.; Hamzeh, Y.; Davoodi, R., Different preparation methods and properties of nanostructured cellulose from various natural resources and residues: A review. *Cellulose.* **2015**, *22*, 935-969. https://doi.org/10.1007/s10570-015-0551-0.

[31] Oliveira, F. B.; Bras, J.; Pimenta, M. T. B.; Curvelo, A. A. S.; Belgacem, M. N., Production of cellulose nanocrystals from sugarcane bagasse fibers and pith. *Ind. Crops Prod.* **2016**, *93*, 48-57. https://doi.org/10.1016/j.indcrop.2016.04.064.

[32] Abraham, E.; Deepa, B.; Pothan, L. A.; Jacob, M.; Thomas, S.; Cvelbar, U.; Anandjiwala, R., Extraction of nanocellulose fibrils from lignocellulosic fibres: A novel approach. *Carbohydr. Polym.* **2011**, *86*, 1468-1475. https://doi.org/10.1016/j.carbpol.2011.06.034.

[33] Neto, W. P. F.; Silverio, H. A.; Dantas, N. O.; Pasquinia, D., Extraction and characterization of cellulose nanocrystals from agro-industrial residue-Soy hulls. *Ind. Crops Prod.* **2013**, *42*, 480-488. https://doi.org/10.1016/j.indcrop.2012.06.041.

[34] Pehlivan, E.; Tran, H. T.; Ouédraogo, W. K. I.; Schmidt, C.; Zachmann, D.; Bahadir, M., Sugarcane bagasse treated with hydrous ferric oxide as a potential adsorbent for the removal of As(V) from aqueous solutions. *Food Chem.* **2013**, *138*, 133-138. https://doi.org/10.1016/j.foodchem.2012.09.110.

[35] Yang, D.; Qiu, L.; Yang, Y., Efficient adsorption of methyl orange using a modified chitosan magnetic composite adsorbent. *J. Chem. Eng. Data.* **2016**, *61*, 3933-3940. https://doi.org/10.1021/acs.jced.6b00706.

[36] Chen, W.; Li, Q.; Cao, J.; Liu, Y.; Li, J.; Zhang, J.; Luo, S.; Yu, H., Revealing the structures of cellulose nanofiber bundles obtained by mechanical nanofibrillation *via* TEM observation. *Carbohydr. Polym.* **2015**, *117*, 950-956. https://doi.org/10.1016/j.carbpol.2014.10.024.

[37] El Achaby, M.; Fayoud, N.; Figueroa-Espinoza, M. C.; Benyoucef, H.; Aboulkas, A., New highly hydrated cellulose microfibrils with a tendril helical morphology extracted from agro waste material:

Application to removal of dyes from waste water. *RSC Adv.* **2018**, *8*, 5212-5224. https://doi.org/10.1039/C7RA10239A.

[38] Buthiyappan, A.; Gopalan, J.; AbdulRaman, A., Synthesis of iron oxides impregnated green adsorbent from sugarcane bagasse: Characterization and evaluation of adsorption efficiency. *J. Environ. Manag.* **2019**, *249*, 109323. https://doi.org/10.1016/j.jenvman.2019.109323.

[39] Alves, M. J.; Cavalcanti, I. V.; de Resende, M. M.; Cardoso, V. L.; Reis, M. H., Biodiesel dry purification with sugarcane bagasse. *Ind. Crops Prod.* **2016**, *89*, 119-127. https://doi.org/10.1016/j.indcrop.2016.05.005.

[40] Maya, S.; Anjali, B., Superabsorbent nanocomposite from sugarcane bagasse, chitin and clay: Synthesis, characterization and swelling behaviour. *Carbohydr. Polym.* **2018**, *193*, 281-288. https://doi.org/10.1016/j.carbpol.2018.04.006.

[41] Brandão, P. C.; Souza, T. C.; Ferreira, C. A.; Hori, C. E.; Romanielo, L. L., Removal of petroleum hydrocarbons from aqueous solution using sugarcane bagasse as adsorbent. *J. Hazard. Mat.* **2010**, *175*, 1106-1112. https://doi.org/10.1016/j.jhazmat.2009.10.060.

[42] Langmuir, I., The adsorption of gases on plane surfaces of glass, mica and platinum. *ACS.* **1918**, *40*, 1361-1403. https://doi.org/10.1021/ja02242a004.

[43] Freundlich, H. M. F., Over the adsorption in solution. *J. Phys. Chem.* **1906**, *57*, 385-470.

[44] Tempkin, M. I.; Pyzhev, V., Kinetics of ammonia synthesis on promoted iron catalyst. *Acta Phys. Chim. USSR.* **1940**, *12*, 327-356.

[45] Dubinin, M. M.; Radushkevich, L. V., The equation of the characteristic curve of the activated charcoal. *Proc. Acad. Sci. USSR Phys. Chem. Sect.* **1947**, *55*, 331-337.

[46] Ojedokun, A. T.; Bello, O. S., Liquid phase adsorption of Congo red dye on functionalized corncobs. *J. Dispersion Sci. Technol.* **2017**, *38*, 1285-1294. https://doi.org/10.1080/01932691.2016.1234384.

[47] Liu, C.; Li, B.; Du, H.; Lv, D.; Zhang, Y.; Yu, G.; Mu, X.; Peng, H., Properties of nanocellulose isolated from corncob residue using sulfuric acid, formic acid, oxidative and mechanical methods. *Carbohydr. Polym.* **2016**, *151*, 716-724. https://doi.org/10.1016/j.carbpol.2016.06.025.

[48] Ferreira, F. V.; Mariano, M.; Rabelo, S. C.; Gouveia, R. F.; Lona, L. M. F., Isolation and surface modification of cellulose nanocrystals from sugarcane bagasse waste: From a micro- to a nano-scale view. *Appl. Surf. Sci.* **2018**, *436*, 1113-1122. https://doi.org/10.1016/j.apsusc.2017.12.137.

[49] Hurtubise, F.; Krassig, H., Classification of fine structural characteristics in cellulose by infrared spectroscopy. *Anal. Chem.* **1960**, *32*, 177-181. https://doi.org/10.1021/ac60158a010.

[50] Nelson, M. L.; O'Connor, R. T., Relation of certain infrared bands to cellulose crystallinity and crystal lattice type. Part 11. A new infrared ratio for estimation of crystallinity in celluloses I and II. *J. Appl. Polym. Sci.* **1964**, *8*, 1325-1341. https://doi.org/10.1002/app.1964.070080322.

[51] Kumar, A.; Negi, Y. S.; Choudhary, V.; Bhardwaj. N. K., Characterization of cellulose nanocrystals produced by acid-hydrolysis from sugarcane bagasse as agro-waste. *J. Mat. Phys. Chem.* **2014**, *2*, 1-8. https://doi.org/10.12691/JMPC-2-1-1.

[52] Kruer-Zerhusen, N.; Cantero-Tubilla, B.; Wilson, D. B., Characterization of cellulose crystallinity after enzymatic treatment using Fourier transform infrared spectroscopy (FTIR). *Cellulose.* **2018**, *25*, 37-48. https://doi.org/10.1007/s10570-017-1542-0.

[53] Zhang, Y.; Tong, D.; Song, K., A comparative analysis on the longitudinal compression characteristics of juvenile and mature northeast Chinese ash (Fraxinus mandshurica Rupr.) subjected to alkaline treatment. *BioResour.* **2013**, *8*, 1963-1975.

[54] Ojo, T. A.; Ojedokun, A. T.; Bello, O. S., Functionalization of powdered walnut shell with orthophosphoric acid for Congo red dye removal. *Particlate Sci. Technol.* **2017**, *37*, 74-85. https://doi.org/10.1080/02726351.2017.1340914.

[55] Moawad, M. N.; El-Sayed, A. A. M.; El-Naggar, N. A., Biosorption of cadmium and nickel ions using marine macrophyte, cymodoceanodosa. *Chem. Ecol.* **2020**, *36*, 458-474..

https://doi.org/10.1080/02757540.2020.1752199.

[56] Suganya, S.; Kumar, P. S.; Saravanan, A.; Rajan, P. S.; Ravikumar, C., Computation of adsorption parameters for the removal of dye from wastewater by microwave assisted sawdust: theoretical and experimental analysis. *Environ. Toxicol. Pharmacol.* **2017**, *50*, 45-57. https://doi.org/10.1016/j.etap.2017.01.014.

[57] Saravanan, A.; Kumar, P. S.; Yaashikaa, P. R.; Kanmani, S.; Varthine, R. H.; Muthu, C. M. M.; Yuvaraj, D., Modelling on the removal of dye from industrial wastewater using surface improved Enteromorpha intestinalis. *Int. J. Environ. Res.* **2019**, *13*, 1-18. https://doi.org/10.1007/s41742-019-00181-0.

[58] Anitha, T.; Kumar, P. S.; Kumar, K. S., Synthesis of nano-sized chitosan blended polyvinyl alcohol for theremoval of Eosin Yellow dye from aqueous solution. *J. Water Proc. Eng.* **2016**, *13*, 127-136. https://doi.org/10.1016/j.jwpe.2016.08.003.

[59] Inyinbor, A. A.; Adekola, F. A.; Olatunji, G. A., Kinetics and isothermal modelling of liquid phase adsorption of Rhodamine B onto urea modified Raphia hookerie epicarp. *Appl. Water Sci.* **2017**, *7*, 3257-3266. https://doi.org/10.1007/s13201-016-0471-7.

[60] Adekola, F. A.; Ayodele, S. B.; Inyinbor, A. A., Efficient rhodamine B removal using acid- and alkaline-activated musa paradisiaca Biochar. *Pol. J. Environ. Stud.* **2019**, *28*, 3063-3070. https://doi.org/10.15244/pjoes/94386.

[61] Bello, O. S.; Alao, O. C.; Alagbada, T. C.; Olatunde, A. M., Biosorption of ibuprofen using functionalized bean husks. *Sustain. Chem. Pharm.* **2019**, *13*, 100151. https://doi.org/10.1016/j.scp.2019.100151.

[62] Ahmad, M. A.; Ahmed, N. B.; Adegoke, K. A.; Bello, O. S., Sorption studies of methyl red dye removal using lemon grass (Cymbopogon citratus). *Chem. Data Collect.* **2019**, *22*, 100249. https://doi.org/10.1016/j.cdc.2019.100249.

[63] Bello, O. S.; Adegoke, K. A.; Sarumi, O. O.; Lameed, O. S., Functionalized locust bean pod (Parkia biglobosa) activated carbon for Rhodamine B dye removal. *Heliyon*. **2019**, *5*, e02323. https://doi.org/10.1016/j.heliyon.2019.e02323.

[64] Adegoke, K. A.; Agboola, O. S.; Ogunmodede, J.; Araoye, A. O.; Bello, O. S., Metal-organic frameworks as adsorbents for sequestering organic pollutants from wastewater. *Mater. Chem. Phys.* **2020**, 253, 123246. https://doi.org/10.1016/j.matchemphys.2020.123246.

[65] Afolabi, I. C.; Popoola, S. I.; Bello, O. S., Modeling pseudo-second-order kinetics of orange peel-paracetamol adsorption process using artificial neural network. *Chemom. Intell. Lab. Syst.* **2020**, S0169-7439(20)30042-3. https://doi.org/10.1016/j.chemolab.2020.104053.

[66] Ahmad, M. A.; Eusoff, M. A.; Oladoye, P. O.; Adegoke, K. A.; Bello, O. S., Statistical optimization of remazol brilliant blue R dye adsorption onto activated carbon prepared from pomegranate fruit peel. *Chem. Data Collect.* **2020**, *28*, 100426. https://doi.org/10.1016/j.cdc.2020.100426.

[67] Afolabi, I. C.; Popoola, S. I.; Bello, O. S., Machine learning approach for prediction of paracetamol adsorption efficiency on chemically modified orange peel. *Spectrochim. Acta A Mol. Biomol. Spectrosc.* **2020**, *243*, 118769. https://doi.org/10.1016/j.saa.2020.118769.

[68] Bello, O. S.; Moshood, M. A.; Ewetumo, B. A.; Afolabi, I. C., Ibuprofen removal using coconut husk activated. *Biomass. Chem. Data Collect.* **2020**, *29*, 100533. https://doi.org/10.1016/j.cdc.2020.100533.

[69] Agboola, O. S.; Bello, O. S., Enhanced adsorption of ciprofloxacin from aqueous solutions using functionalized banana stalk. *Biomass Convers. Biorefin.* **2020**. https://doi.org/10.1007/s13399-020-01038-9.

[70] Ahmad, M. A.; Ahmed, N.; Adegoke, K. A.; Bello, O. S., Trapping synthetic dye molecules using modified lemon grass adsorbent. *J. Dispers. Sci. Technol.* **2020**. https://doi.org/10.1080/01932691.2020.1844016.

[71] Bello, O. S.; Alao, O. C.; Alagbada, T. C.; Agboola, O. S.; Omotoba, O. T.; Abikoye, O. R., A renewable, sustainable and low-cost adsorbent for ibuprofen removal. *Water Sci. Technol.* **2021**.

https://doi:10.2166/wst.2020.551.

[72] Ahmad, M. A.; Ahmed, N. B.; Adegoke, K. A.; Bello, O. S., Adsorptive potentials of lemongrass leaf for methylene blue dye removal. *Chem. Data Collect.* **2021**, *31*, 100578. https://doi.org/10.1016/j.cdc.2020.100578.

[73] Bello, O. S.; Alagbada, T. C.; Alao, O. C.; Olatunde, A. M., Sequestering a non-steroidal anti-inflammatory drug using modified orange peels. *Appl. Water Sci.* **2020**, *10*, 172. https://doi.org/10.1007/s13201-020-01254-8.

[74] Bello, O. S.; Adegoke, K. A.; Fagbenro, S. O.; Lameed, O. S., Functionalized coconut husks for rhodamine-B dye sequestration. *Appl. Water Sci.* **2019**, *9*, 189. https://doi.org/10.1007/s13201-019-1051-4.

[75] Bello, O. S.; Alabi, E. O.; Adegoke, K. A.; Adegboyega, S. A.; Inyinbor, A. A.; Dada, A. O., Rhodamine B dye sequestration using Gmelina aborea leaf powder. *Heliyon.* **2019**, *5*, e02872. https://doi.org/10.1016/j.heliyon.2019.e02872.

[76] Sun, B.; Yuan, Y.; Li, H.; Li, X.; Zhang, C.; Guo, F.; Liu, X.; Wang, K.; Zhao, X. S.,Waste-cellulose-derived porous carbon adsorbents for methyl orange removal. *Chem. Eng. J.* **2019**, *371*, 55-63. https://doi.org/10.1016/j.cej.2019.04.031.

[77] Zhai, L.; Bai, Z.; Zhu, Y.; Wang, B.; Luo, B., Fabrication of chitosan microspheres for efficient adsorption of methyl orange. *Chinese J. Chem. Eng.* **2018**, *26*, 657-666.https://doi.org/10.1016/j.cjche.2017.08.015.